JOURNAL OF MATERIALS SCIENCE 32 (1997) 3759–3764

# Microstructural investigation of Bi–Sr–Ca–Cu–oxide thick films on alumina substrates

J. A. ALARCO*, A. ILUSHECHKIN*, T. YAMASHITA*, A. BHARGAVA*, J. BARRY, I. D. R. MACKINNON*
*Centre for Microscopy and Microanalysis, The University of Queensland, Queensland 4072, Australia*

The microstructure of Bi–Sr–Ca–Cu–oxide (BSCCO) thick films on alumina substrates has been characterized using a combination of X-ray diffractometry, scanning electron microscopy, transmission electron microscopy of sections across the film/substrate interface and energy-dispersive X-ray spectrometry. A reaction layer formed between the BSCCO films and the alumina substrates. This chemical interaction is largely responsible for off-stoichiometry of the films and is more significant after partial melting of the films. A new phase with fcc structure, lattice parameter $a = 2.45$ nm and approximate composition $Al_3Sr_2CaBi_2CuO_x$ has been identified as reaction product between BSCCO and $Al_2O_3$.

## 1. Introduction

Polycrystalline alumina ($Al_2O_3$) substrates are extensively used in thick-film technology for electronic applications because they fulfil most of the general requirements for a good substrate material [1]. The required properties include high values of electrical resistivity, mechanical strength, thermal shock resistance and thermal conductivity, and low values of dielectric constant and dielectric loss. The substrates should also be very refractory and cost should be reasonable. Thick films are normally produced by screen-printing and include different elements with dielectric, resistive, semiconducting and conducting properties, respectively. These elements are often combined with discrete components into a hybrid circuit. In addition to the general requirements for a substrate material, other properties such as power rating and composition are important, depending on the particular application and the nature of the ink or paste. Thick films may also be produced by a doctor-blade processing technique.

Within the field of superconductivity, thick films are under development for application in microwave components (e.g. filters, antennae and wide-band delay lines) and in instrumentation for nuclear magnetic resonance (NMR) or magnetic resonance imaging (MRI). Though several substrate materials can be used for superconducting thick films, it is highly desirable to adjust their processing parameters to standard substrate materials (and firing procedures) compatible with already existent thick-film technology such as alumina substrates.

In this work, the microstructure of Bi–Sr–Ca–Cu–oxide (BSCCO) thick films (processed by the doctor-blade technique) on alumina substrates have been characterized using a combination of X-ray diffractometry, scanning electron microscopy (SEM), transmission electron microscopy (TEM) and energy-dispersive X-ray spectrometry (EDX). Particular attention has been paid to the BSCCO/alumina interface. This work is part of a larger study aimed at the development of BSCCO inks or pastes for optimum thick-film properties on bare or buffered alumina substrates.

## 2. Experimental procedure

The alumina substrates are of the type normally used within the electronic industry. They are porous (about 93% of theoretical density as determined from sample weight and dimensions) and contain a small percentage of magnesium, silicon and calcium impurities. A description of the BSCCO pastes and thick-film preparations is in preparation for separate publication [2]. Briefly, high-quality BSCCO powder is prepared by a co-precipitation method described by Bhargava *et al.* [3]. Pure BSCCO powder or powder mixed with different percentages of silver powder (in the range 5–20 wt%) are mixed with an organic medium. The organic medium consists of a mixture of ethyl cellulose, butyl acetate and terpineol in suitable amounts so as to achieve the desired viscosity. The pastes are doctor-blade processed on to alumina substrates and dried in air at 130–150 °C for 30 min. After drying, the thick films are sintered (or partially melted) in a tube furnace (in air) at 830–960 °C for 10 min. The heating and cooling rates were about 40–50 °C $min^{-1}$. Three thick films have been selected for TEM microstructural

* Also at UniQuest Ltd.

0022–2461  

investigation. The nominal compositions for the respective pastes were $Bi_{2.0}Sr_{2.1}Ca_{0.9}Cu_2O_x$ (film A), $Bi_{2.0}Sr_{2.1}Ca_{0.9}Cu_2O_x + 10\,wt\%$ Ag (film B) and $Bi_{1.65}Pb_{0.35}Sr_{1.6}Ca_2Cu_3O_x + 20\,wt\%$ Ag (film C). (These compositions will be referred to as 2212, 2212 + 10% Ag, and 2223 + 20% Ag, respectively, from now on). Films A, B and C have been partially melted at 890, 888 and 860 °C, respectively.

Microstructures were characterized using a Siemens X-ray diffractometer with a D5000 goniometer and $CuK_\alpha$ radiation, a Jeol 6400F field-emission SEM and a Jeol 4000FX TEM, both equipped with Link EDX spectrometers. TEM samples were prepared using standard cross-section techniques, such as grinding, dimple-polishing and argon ion milling. The ion milling was carried out in a Gatan Duo Mill using argon ions with 4.5 keV incident at 10°–15°, and a cold stage. A glass shield protected the sample cross-section from bombardment from the film side at all times. An opening of about 120 °C allowed argon milling from the substrate side. In this way, the substrate partially shadowed the film from direct bombardment, and milling of the substrate was the rate-limiting step. Conditions were changed to 2.5 keV and 10° during the final period (about 1 h) of ion milling. Samples were allowed to equilibrate to room temperature for at least 1 h before opening the chamber of the ion mill in order to avoid condensation of water vapour from the air.

## 3. Results

### 3.1. Thick films prepared from 2212 paste

Detailed X-ray diffraction analyses have been carried out on these samples as well as a larger set of samples and heat-treatment conditions, however, only relevant phase-identification data are summarized here. The powders, as well as the dried thick films (before sintering/partial melting), consist primarily of 2212 phase as determined by X-ray diffractometry. After sintering at 880 °C (below the melting temperature ~883 °C), only pure 2212 phase is detected. The film is highly porous and adhesion to the substrate is poor in this case. After partial melting at 885 °C or higher, a mixture of 2201 and 2212 phases appears. Minor amounts of (Sr, Ca)$CuO_x$ phase are also detected [4–7]. The amounts of 2201 and (Sr, Ca)$CuO_x$ phases and the degree of film orientation increase with increasing temperature above the melting temperature. The density, as well as film adhesion, are significantly improved after partial melting. Addition of silver to the powder lowers the partial melting temperatures about 17 °C. Similar X-ray results on phase abundance and degree of film orientation are observed with silver addition to the paste, but with a shift toward lower temperatures.

Film A contained several (Sr, Ca)$CuO_x$ inclusions within the BSSCO matrix as determined using SEM (Fig. 1a). The inclusions are relatively equiaxed and up to about 10 μm in diameter. Film B (2212 + 10% Ag) contains irregularly shaped silver inclusions in addition to the (Sr,Ca)$CuO_x$ inclusions (Fig. 1b). A reaction layer (about 2–3 μm thick) forms between the

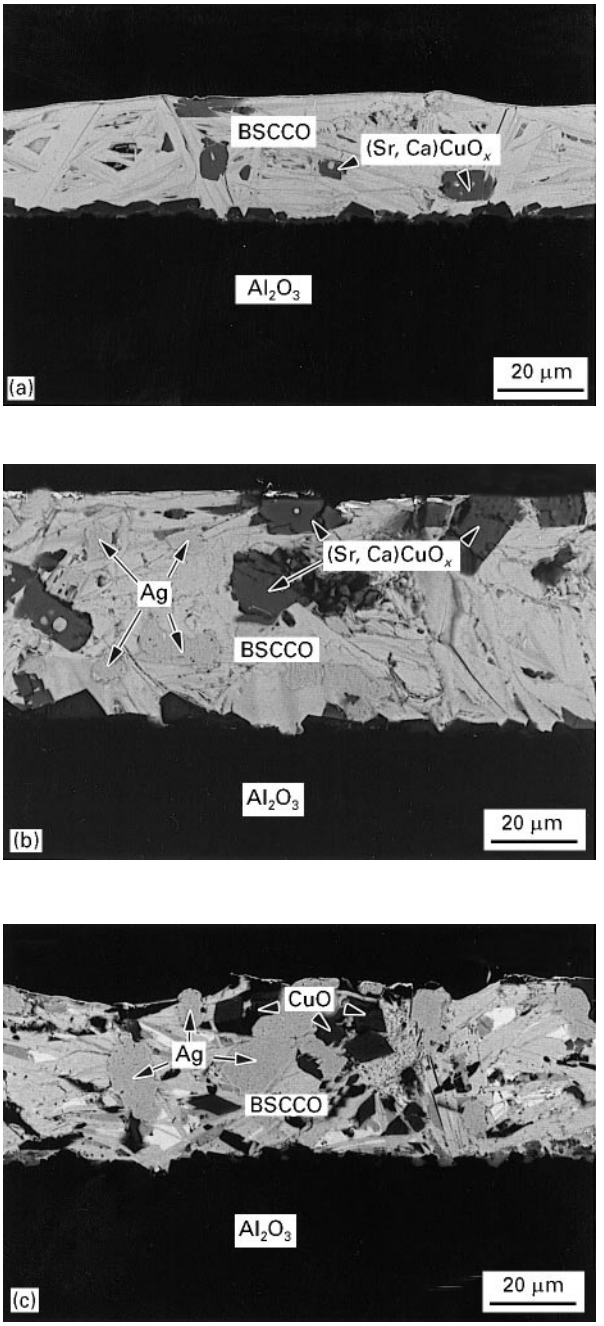


*Figure 1* Scanning electron micrographs using backscattered electrons of films (a) A, (b) B and (c) C. The major phases present are indicated. The regions in brightest contrast in (c) are bismuth-rich (probably bismuth-oxide).

BSCCO film and the $Al_2O_3$ substrate (Fig. 1a and b). The boundary between the film and the reaction layer is highly faceted while the reaction front into the $Al_2O_3$ substrate is very wavy and irregular. The reaction is significant when partial melting occurs. SEM also shows that the alumina substrates are highly porous (about 6% porosity), and that microcracks exist in the interior of the BSCCO films.

The grains of the BSCCO films are characterized by a high density of intergrowths and twin domains. Fig. 2a shows a representative example of 2212 and 2201 intergrowths, while Fig. 2b shows twin domains in a 2201 grain (both in film A). The twin domains are typical of the BSCCO phases [8, 9] and correspond to a 90° rotation around the *c*-axis (directions are

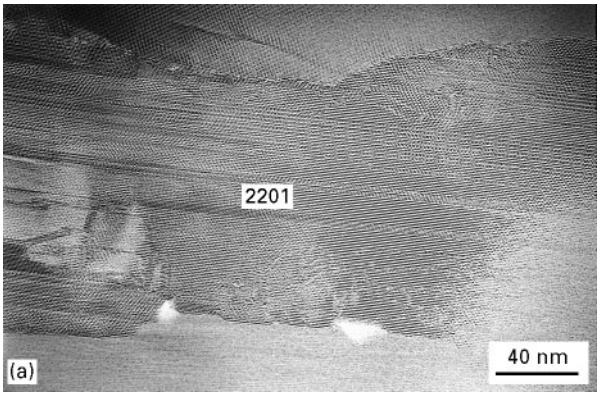


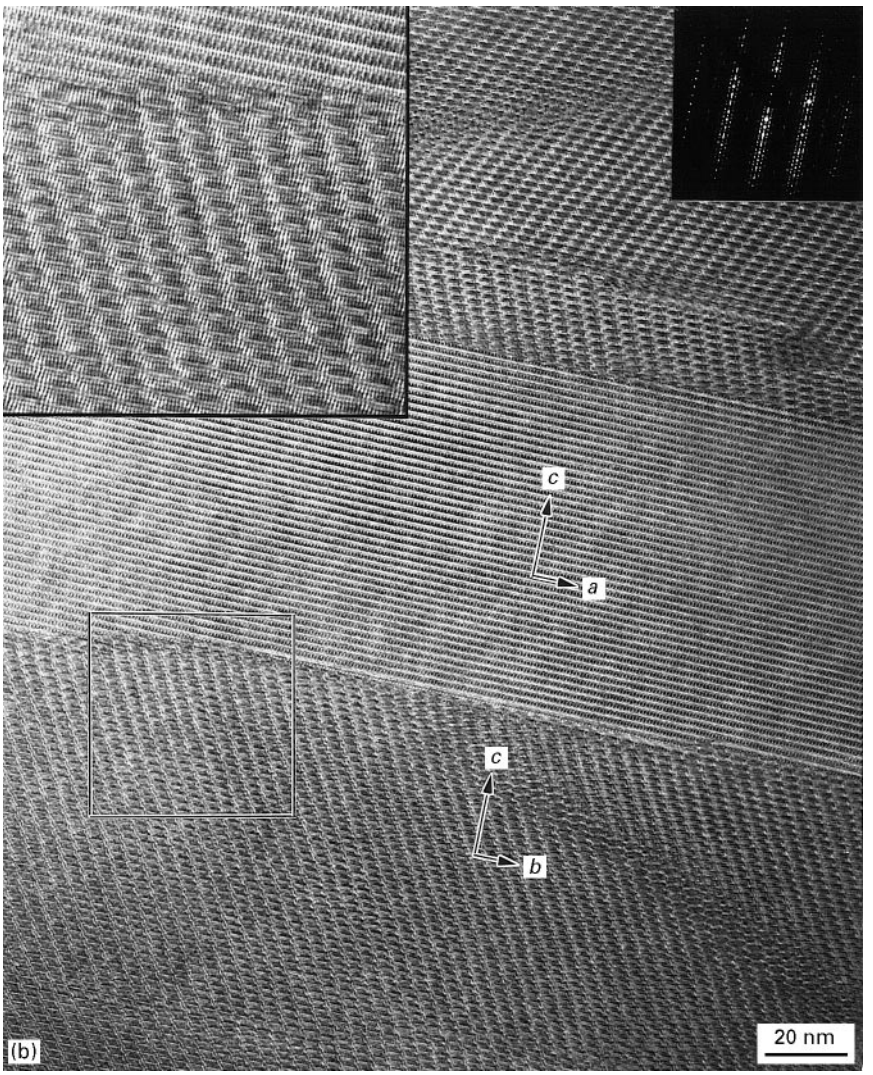


*Figure 2* (a) Transmission electron micrograph showing a typical 2201-BSCCO grain (in film A) with characteristic high density of stacking defects and intergrowths. (b) Transmission electron micrograph of twin domains (slightly deviated from the exact twin relation) in 2201 (directions are indicated in the figure). The inserts show a diffraction pattern from the three twin variants and a magnified view of the region within the rectangle, respectively.

indicated in Fig. 2b). Twin boundaries are relatively straight when perpendicular to the common *c*-axis direction and wavy for other geometries. In addition, grains projected along the *a*-direction display a typical incommensurate modulation of the lattice [8–10], as can be seen for the twin domain in Fig. 2b (see insert). Most of the grain boundaries are clean and show long straight facets. However, small pockets and thin wetting layers of an amorphous secondary phase have been identified at triple junctions and their adjacent grain boundaries, respectively. A significant amount of microcracking is detected in the BSCCO films. However, it is likely that some enhancement of microcracking occurs during TEM specimen preparation.

The reaction layer that forms between the BSCCO film and the $Al_2O_3$ substrate consists mainly of an Al–Sr–S–oxide phase (as determined using EDX) with

cubic structure and lattice parameter $a = 1.85$ nm (identified using electron diffraction). This phase was identified as $Sr_4Al_6O_{12}SO_4$ (JCPDS 30-1278) from electron diffraction data in combination with EDX compositional information. The origin of the sulphur has not yet been clearly established. However, it is probable that sulphur is a component of an impurity phase in the substrates or that it is absorbed during a cleaning step in sulphuric acid. The thickness of the reaction layer is about 2–3 μm. The boundary between the film and the reaction layer is highly faceted with straight facets typically ranging from a few hundred nanometres up to 2–3 μm in length. However, no specific high-density lattice plane of the film is apparently parallel to the facets at the film/reaction layer interface (see Fig. 3). On the other hand, the reaction front into the $Al_2O_3$ substrate is very wavy and irregular. The reaction layer also contains fine-grained material (<200 nm diameter), predominantly at the wavy reaction front. Calcium segregation is detected by EDX at the wavy reaction front between the $Sr_4Al_6O_{12}SO_4$ grains and the $Al_2O_3$ substrate. The BSCCO film in the vicinity of the alumina substrate surface is not highly oriented (with its *c*-axis direction perpendicular to the substrate surface) (see Fig. 3). This suggests that the degree of *c*-axis orientation implied by X-ray diffraction results occurs predominantly at the film surface.

Apart from the presence of irregularly shaped silver inclusions, the microstructure of film B (2212 + 10% Ag paste) does not differ significantly from that of film A. The reaction layer appears slightly thicker (about 2.5–3 μm) in film B than in film A, and a slight increase in the number of small amorphous pockets and wetting layers is detected. These observations are consistent with the reduction of melting temperature (increase in amount of liquid phases) with silver addition. The observation of a small pocket and thin wetting layers of an amorphous secondary phase at a triple junction and the phase boundaries adjacent to a silver inclusion, respectively, provides further evidence for this interpretation (see Fig. 4). A transmission electron micrograph of a silver inclusion surrounded by (Sr, Ca)$CuO_x$ is shown in Fig. 4. The same crystalline region, as determined from diffraction contrast imaging, shows varying strontium and calcium contents at different locations. The Cu/(Sr + Ca) peak intensity ratio varied in the range 1.1–1.4.

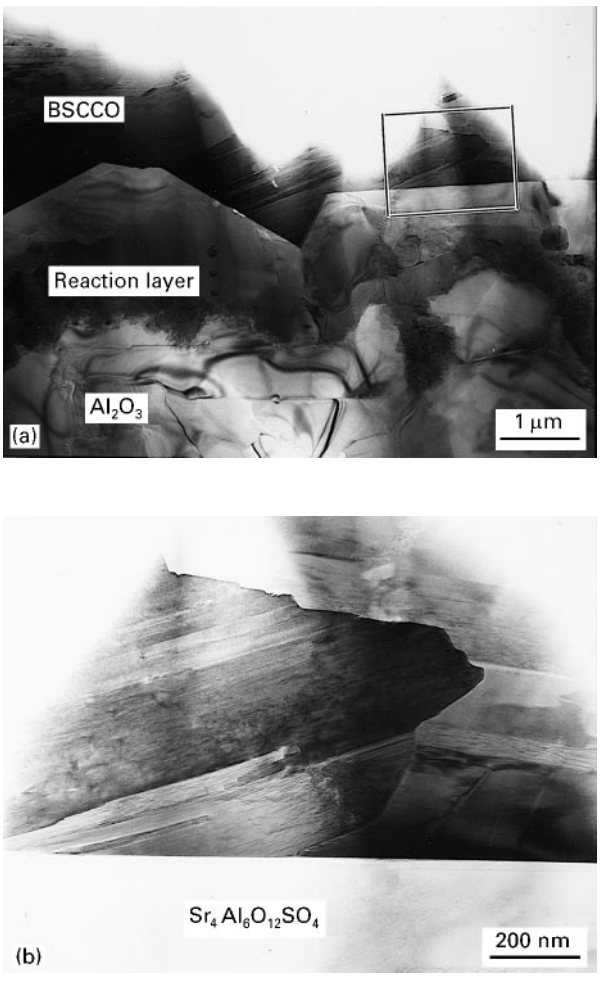


*Figure 3* (a) Transmission electron micrograph of a section across the BSCCO film/alumina substrate interface in film A. A reaction layer (labelled) has formed between the film and the substrate. Note that the interface between the film and the reaction layer is highly faceted. (b) A magnified view of the region within the rectangle shown in (a). High density lattice planes of the thick film are apparently not parallel to the faceted interface.

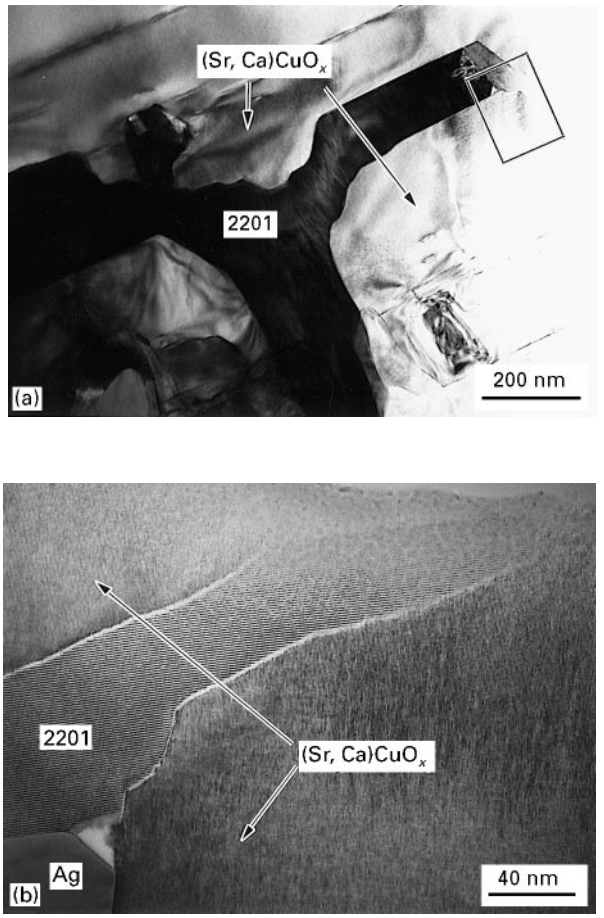


*Figure 4* Transmission electron micrographs of a silver inclusion surrounded by 2201 and (Sr, Ca)$CuO_x$ phases. (b) A magnified view of the region within the rectangle shown in (a). The presence of the silver inclusion has influenced the morphology of the adjacent 2201 grains. Note the amorphous pocket and intergranular secondary phases adjacent to the silver inclusion.

### 3.2. Thick films prepared from 2223 paste

Even though the stoichiometry of this powder is close to 2223, 2223 phase has not been formed at any stage of the powders, the pastes or the thick films preparations. The powders, as well as the dried thick films (before sintering/partial melting), consist primarily of 2212 phase as determined using X-ray diffractometry. The 2223 paste does not melt in the range 830–960 °C without silver addition, but with silver addition, partial melting begins at about 836 °C. After sintering below the melting temperature, only pure 2212 phase is detected. After sintering above the melting temperature (i.e. after partial melting), the thick film consists of a mixture of 2212 and 2201 phases. Minor amounts of (Sr, Ca)$CuO_x$ phase, (Sr, Ca)$Cu_2O_x$ phase [4–7] and $Ca_2CuO_3$ are also detected. The amount of 2201 and the degree of film orientation also increases with increasing temperature, until the 2212 phase eventually disappears. However, the amount of other phases detected by X-ray diffractometry does not vary systematically with increasing temperature. The behaviour of the film density and film adhesion below and above the melting temperature is similar to the aforementioned 2212 case.

In film C (2223 + 20% Ag paste), several pronounced changes in the microstructure take place as characterized using SEM and TEM. This film contains a larger variety of secondary phases such as $Ca_2CuO_3$, CuO, bismuth-rich phase (probably bismuth-oxide). Most inclusions within the BSCCO matrix are CuO in this case (Fig. 1c).

Large grains of $Al_2SrCa_2O_6$ and $Ca_2CuO_3$ are present in the reaction layer and its vicinity, respectively (Fig. 5). Small grains of another phase with typical square or rectangular morphology are also found in the reaction layer (see Fig. 6). The small grain sizes typically range between a few tens and 200 nm diameter. Regions of small grains also appear surrounded by BSCCO phases (2201 and 2212) in the interior of the film adjacent to the reaction layer, so that direct connection of these aluminium-rich regions to the substrate is not always apparent. These small grains correspond to an fcc structure with lattice parameter $a = 2.45$ nm as determined using electron diffraction. The approximate composition of this phase is $Al_3Sr_2CaBi_2CuO_x$ as determined using EDX. A JCPDS standard file is not known for this compound. These data suggest that this material in the interface region is a new phase.

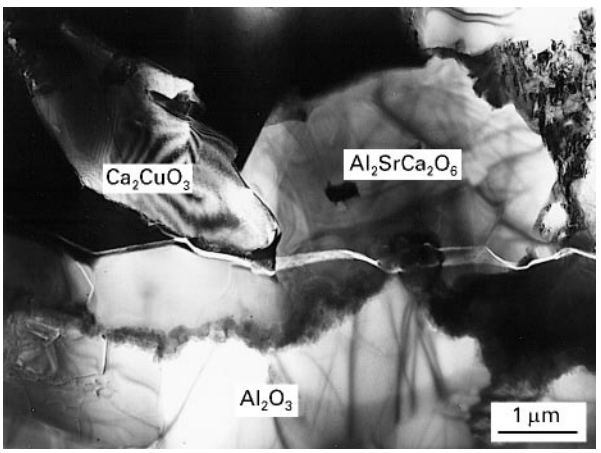


*Figure 5* Transmission electron micrograph of a section across the BSCCO film/alumina substrate interface in film C (2223 + 20% Ag). A large grain of $Ca_2CuO_3$ near the film/substrate interface is indicated. The reaction layer consists mostly of $Al_2SrCa_2O_x$ in this case.

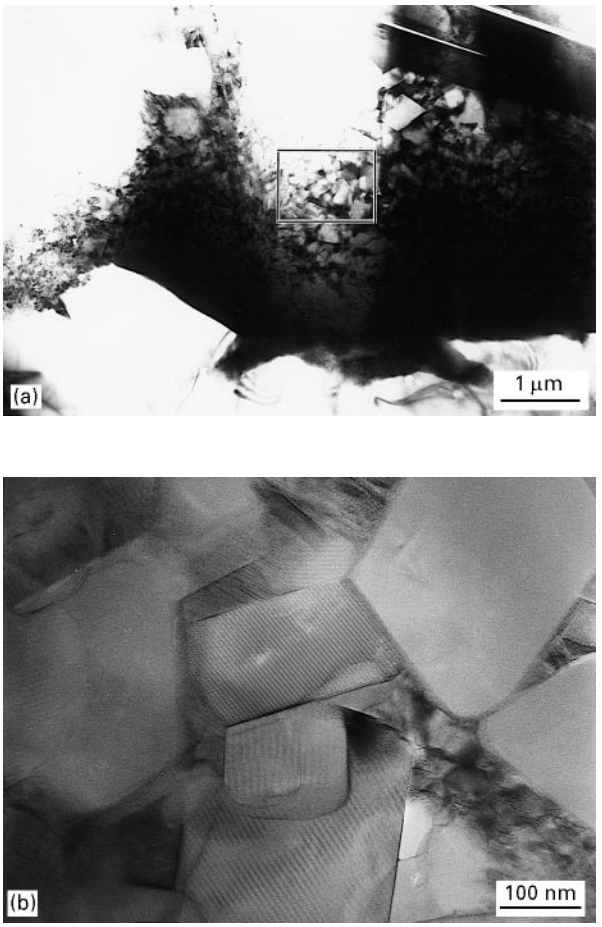


*Figure 6* Transmission electron micrographs of fine-grained phase with typical rectangular morphology, which is a product of the reaction between BSCCO and $Al_2O_3$. This phase has an fcc structure, lattice parameter $a = 2.45$ nm, and approximate composition $Al_3Sr_2CaBi_2CuO_x$. (b) A magnified view of a region similar to the region within the rectangle shown in (a).

## 4. Discussion

SEM and TEM results show that different phases which are not detectable by X-ray diffractometry may be present at different film thicknesses. This apparent incongruity is due to the depth of information for the X-ray technique and to the effects of relative orientation of phases in the thick film. Therefore, X-ray diffractometry results are not, in general, representative of the entire film thickness. This observation also applies to the degree of *c*-axis orientation (perpendicular to the substrate surface) obtained during partial melting, which is apparently higher at the film free surface.

Reaction between the BSCCO film and the alumina substrate is significant at temperatures corresponding to the beginning of melting (and higher) and it is largely responsible for off-stoichiometry of the final

film composition. Good adhesion is also related to the chemical interaction between the BSCCO film and the alumina substrate. Partial melting is required for densification and texture improvement (as well as good adhesion), but it is invariably associated with a reduction in the amount of the 2212 phase present. This factor precludes testing of superconducting properties within our laboratory which is limited to liquid-nitrogen temperatures. It is likely that the off-stoichiometric composition produced by the reaction of the partially melted BSCCO film with the alumina substrate inhibits the solidification of 2212 from the partial melt during cooling. In addition, relatively fast cooling rates (about 40–50 °C $min^{-1}$) are used to avoid further reaction between the BSCCO film and the alumina substrate (and because these heating/cooling rates are commonly used in thick-film technology for the electronic industry). Such cooling rates quickly bring the temperature of the partial melt into the stability range for the solidification of 2201, without allowing enough time in the stability range for the solidification of 2212 [4, 5, 7]. Compensation of the composition, taking into account the reaction between the BSCCO film and the alumina substrate, is a possible solution for the control of stoichiometry of the final film. However, the presence of cations in excess of 2212 may enhance other reactions with the substrate instead, as is observed for the paste of 2223 composition with silver addition.

This work shows the need for dense, non-porous buffer layers with good adhesion on alumina, that are relatively inert to BSCCO. However, similar concerns regarding adhesion of BSCCO to the buffer layer, which may require a small degree of interaction with the thick film, also arise. Further work is aimed at testing silver as a buffer layer on polycrystalline alumina substrates.

## 5. Conclusion

A reaction occurs between BSCCO film and alumina substrate, and is largely responsible for off-stoichiometry of the BSCCO thick films. A good adhesion is associated with this chemical interaction. Partial melting is required for densification and improvement of the texture of BSCCO films. However, partial melting enhances the reaction between BSCCO and alumina. The reaction of the partially melted BSCCO film with the alumina substrate hinders the solidification of 2212 from the partial melt. A new phase with approximate composition $Al_3Sr_2CaBi_2CuO_x$, fcc structure and lattice parameter $a = 2.45$ nm has been identified as a product of the reaction between BSCCO and $Al_2O_3$.


## Acknowledgement

Financial support from The University of Queensland is gratefully acknowledged.


## References


1. R. W. WEST, in "Ceramic materials for electronics – processing, properties and applications", edited by R. C. Buchanan (Marcel Dekker, New York, 1991) pp. 435–88.
2. A. ILUSHECHKIN, T. YAMASHITA, J. A. ALARCO and I. D. R. MACKINNON, *Super cond. Sci. and Technol.* (1997) in press.
3. A. BHARGAVA, T. YAMASHITA and I. D. R. MACKINNON, *Phys. C* **247** (1995) 385.
4. J. POLONKA, M. XU, Q. LI, A. I. GOLDMAN and D. K. FINNEMORE, *Appl. Phys. Lett.* **59** (1991) 3640.
5. T. HASEGAWA, T. KITAMURA, H. KOBAYASHI, H. KUMAKURA, H. KITAGUCHI and K. TOGANO, *ibid.* **60** (1992) 2692.
6. D. P. MATHEIS, S. T. MISTURE and R. L. SNYDER, *Phys. C* **217** (1993) 319.
7. T. HASEGAWA, H. KOBAYASHI, H. KUMAKURA, H. KITAGUCHI and K. TOGANO, *ibid.* **222** (1994) 111.
8. G. VAN TENDELOO, H. W. ZANDBERGEN, J. VAN LANDUYT and S. AMELINCKX, *Appl. Phys. A* **46** (1988) 153.
9. O. EIBL, *Phys. C* **168** (1990) 239.
10. H. W. ZANDBERGEN, W. A. GROEN, F. C. MIJLHOFF, G. VAN TENDELOO and S. AMELINCKX, *ibid.* **156** (1988) 325.



*Received 4 December 1995*
*and accepted 10 February 1997*